Experimental Study of the Interplay between Long-Range Electron Transfer and Redox Probe Permeation at Self-Assembled Monolayers: Evidence for Potential-Induced Ion Gating

ARTICLE *in* JOURNAL OF THE AMERICAN CHEMICAL SOCIETY · JUNE 2005

Impact Factor: 12.11 · DOI: 10.1021/ja050265j · Source: PubMed

J|A|C|S
ARTICLES
Published on Web 04/12/2005

Experimental Study of the Interplay between Long-Range Electron Transfer and Redox Probe Permeation at Self-Assembled Monolayers: Evidence for Potential-Induced Ion Gating

Juan José Calvente,*,† German López-Pérez,† Pablo Ramírez,† Héctor Fernández,‡ María Alicia Zón,‡ Willem H. Mulder,§ and Rafael Andreu*,†

Contribution from the Departamento de Quimica Fisica, Facultad de Quimica, Universidad de Sevilla, 41012, Sevilla, Spain, Departamento de Quimica, Facultad de Ciencias Exactas, Fisico-Quimicas y Naturales, Universidad Nacional de Rio Cuarto, Agencia Postal No 3, 5800 Rio Cuarto, Argentina, and Department of Chemistry, University of the West Indies, Mona Campus, Kingston 7, Jamaica

Received January 14, 2005; E-mail: pacheco@us.es; fondacab@us.es

Abstract: Evidence for the competition between long-range electron transfer across self-assembled monolayers (SAMs) and incorporation of the redox probe into the film is reported for the electroreduction of $Ru(NH_3)_6^{3+}$ at hydroxyl- and carboxylic-acid-terminated SAMs on a mercury electrode, by using electrochemical techniques that operate at distinct time scales. Two limiting voltammetric behaviors are observed, consistent with a diffusion control of the redox process at mercaptophenol-coated electrodes and a kinetically controlled electron transfer reaction in the presence of neutral $HS-(CH_2)_{10}-COOH$ and $HS-(CH_2)_n-CH_2OH$ (n = 3, 5, and 10) SAMs. The monolayer thickness dependence of the standard heterogeneous electron transfer rate constant shows that the electron transfer plane for the reduction of $Ru(NH_3)_6^{3+}$ at hydroxyl-terminated SAMs is located outside the film | solution interface at short times. However, long time scale experiments provide evidence for the occurrence of potential-induced gating of the adsorbed structure in some of the monolayers studied, which takes the form of a chronoamperometric spike. Redox probe permeation is shown to be a kinetically slow process, whose activation strongly depends on redox probe concentration, applied potential, and chemical composition of the intervening medium. The obtained results reveal that self-assembled monolayers made of mercaptobutanol and mercaptophenol preserve their electronic barrier properties up to the reductive desorption potential of a fully grown SAM, whereas those of mercaptohexanol, mercaptoundecanol, and mercaptoundecanoic acid undergo an order/disorder transition below a critical potential, which facilitates the approach of the redox probe toward the electrode surface.

Introduction

Understanding long-range electron transfer reactions is of crucial importance to unravel the workings of biological systems and to design molecular electronic devices.[1,2] Three general approaches have been developed to elucidate the role of the intervening medium in mediated electron transfer reactions. The first strategy involves the study of photoinduced electron transfers between donor/acceptor pairs linked by synthetic molecular bridges or in purposely modified metalloproteins.[3] In the second approach, the electron tunneling current between an electrode and a redox probe separated by an organized film is measured.[4,5] The redox species can be either covalently linked to the film or freely diffusing in the solution. The third strategy makes use of solid-state metal−insulator−metal junctions to probe the electron transport across the sandwiched molecular spacer.[6] The main goal of the present work is to explore the interplay between the two charge transfer processes that are

† Universidad de Sevilla.
‡ Universidad Nacional de Rio Cuarto.
§ University of the West Indies.

(1) (a) Tour, J. M. *Acc. Chem. Res.* **2000**, *33*, 791. (b) Ratner, M. *Nature* **2000**, *404*, 6774. (c) Rueckes, T.; Kim, K.; Joselevich, E.; Tsen, G. Y.; Cheung, C.-L.; Lieber, C. M. *Science* **2000**, *289*, 5476. (d) Fox, M. A. *Acc. Chem. Res.* **1999**, *32*, 201.
(2) (a) McLendon, G. *Acc. Chem. Res.* **1988**, *21*, 160. (b) Gray, H. B.; Winkler, J. B. *Annu. Rev. Biochem.* **1996**, *65*, 537. (c) Kelley, S. O.; Barton, J. K. *Science* **1999**, *283*, 375. (d) Page, C. C.; Moser, C. C.; Chen, X.; Dutton, P. L. *Nature* **1999**, *402*, 47.
(3) (a) Winkler, J. R.; Gray, H. B. *Chem. Rev.* **1992**, *92*, 369. (b) Paddon-Row, M. N. *Acc. Chem. Res.* **1994**, *27*, 18. (c) Langen, R.; Chang, I.-J.; Germanas, J. P.; Richards, J. H.; Winkler, J. R.; Gray, H. B. *Science* **1995**, *268*, 1733. (d) Davis, W. B.; Svec, W. A.; Ratner, M. A.; Wasielewski, M. R. *Nature* **1998**, *396*, 60.
(4) Finklea, H. O. In *Electroanalytical Chemistry*; Bard, A. J., Rubinstein, I., Eds.; Marcel Dekker: New York, 1996; Vol. 19, pp 109−335.
(5) (a) Chidsey, C. E. D. *Science* **1991**, *251*, 919. (b) Hanshew, D. D.; Finklea, H. O. *J. Am. Chem. Soc.* **1992**, *114*, 3173. (c) Finklea, H. O.; Liu, L.; Ravenscroft, M. S.; Punturi, S. *J. Phys. Chem.* **1996**, *100*, 18852. (d) Sachs, S. B.; Dudek, S. P.; Hsung, R. P.; Sita, L. R.; Smalley, J. F.; Newton, M. D.; Feldberg, S. W.; Chidsey, C. E. D. *J. Am. Chem. Soc.* **1997**, *119*, 10563. (e) Weber, K.; Hockett, L.; Creager, S. E. *J. Phys. Chem. B* **1997**, *101*, 8286. (f) Smalley, J. F.; Finklea, H. O.; Chidsey, C. E. D.; Linford, M. R.; Creager, S. E.; Ferraris, J. P.; Chalfant, K.; Zawodzinsk, T.; Feldberg, S. W.; Newton, M. D. *J. Am. Chem. Soc.* **2003**, *125*, 2004. (g) Liu, B.; Bard, A. J.; Mirkin, M. V.; Creager, S. E. *J. Am. Chem. Soc.* **2004**, *126*, 1485.

10.1021/ja050265j CCC: $30.25

envisaged to operate whenever a freely diffusing redox species encounters an appropriately polarized monolayer-coated electrode, namely, long-range electron transfer and ion permeation across the film.

The use of electrodes coated with blocking self-assembled monolayers (SAMs) allowed Miller et al.[7] and Xu et al.[8] to determine the redox kinetics of freely diffusing redox couples at high overpotentials, which were previously unattainable at bare electrodes due to mass-transport limitations. Electron transfer rate constants were shown to vary with overpotential according to predictions based on Marcus density-of-states (DOS) theory. Cheng et al.[9] have explored the characteristics of the donor/acceptor electronic coupling across self-assembled monolayers. They reported that introduction of an ether, olefin, or alkyne functionality in the interior of ω-hydroxyalkanethiol monolayers results in a decrease of the electron transfer rate between the electrode and the redox probe, in agreement with quantum mechanical predictions.[9,10] On the other hand, an increase of the tunneling current has been observed when an amide group was introduced in the hydrocarbon backbone of the monolayer[11] or in the center of a bilayer barrier forming a tunneling junction between two mercury electrodes.[6b] In the case of chemical modification of the outer part of the monolayer, interpretation of kinetic effects requires a precise knowledge of the location of the redox probe at the film | solution interface. Miller et al.[7b] ascribed the increase of the tunneling current for ferricyanide electroreduction at ω-hydroxyalkanethiol-coated gold electrodes, as compared to that observed at methyl-terminated SAMs, to a closer approach of the redox species to the hydroxylated monolayer surface due to its more hydrophilic character. Slowinski et al.[12] proposed the use of the reorganization energy and the maximum value of the electron transfer rate constant as diagnostic parameters to locate the electron transfer plane, inside or outside of the monolayer, based on their dependence on the dielectric permittivity profile.

The electrochemical properties of SAMs have been mainly studied at solid substrates, but additional advantages can be taken from the use of a mercury drop electrode. Its atomically smooth surface facilitates the formation of defect-free, closely packed monolayers,[13,14] while the possibility of expanding or contracting its surface area allows for a gradual variation of the molecular tilt angle[15,16] or the interconversion of adsorbed structures with distinct surface density.[17] Majda et al.[16] studied the tunneling barrier properties of methyl- and hydroxyl-terminated SAMs on mercury by using both native and expanded films in the presence of a redox probe. The small increase of the tunneling current observed upon expanding the electrode surface area led them to conclude that, in addition to the dominant through-bond electronic coupling, there exists a less efficient tunneling pathway involving a chain-to-chain coupling (through-space coupling). In a more recent study, Yamamoto and Waldeck[18] extended this parallel pathways model by allowing for multiple interchain jumps and applied it to provide a better description of tunneling currents measured across high tilt-angle monolayers. Additional studies have demonstrated that the contribution of the interchain coupling pathway depends on the chemical composition of the molecular spacer and the location of the redox group in the SAM.[5c,9−11,19,20] Apart from their use in studying long-range electron transfer reactions, freely diffusing redox species can also be employed to probe the state of adsorbed molecules during the self-assembly process. The sensitivity of the hexammine−ruthenium(III) reduction rate to its separation from the electrode surface allowed us to identify two adsorbed states during the formation of a 6-mercaptohexanol SAM on a hanging mercury drop electrode.[17]

As mentioned earlier, an aspect that requires special consideration in the kinetic analysis of redox probes at coated electrodes is the possible incorporation of ions into the monolayer as the overpotential is increased. Evidence for ion permeation into short alkanethiol SAMs was inferred by Porter et al.[21] from the dependence of the electrode differential capacitance on the hydrocarbon chain length and nature of supporting electrolyte. More recently, Boubour and Lennox[22] have studied the ionic insulating properties of various alkanethiol-based SAMs in the absence of redox active species by using impedance spectroscopy. From the analysis of the low-frequency response, they reported the existence of a critical potential, below which the adsorbed film becomes permeable to ions from solution. The critical potential was shown to shift toward more negative values as the chain length of the adsorbed thiol was increased. Later, Protsalio and Fawcett[23] extended this type of study to propylene carbonate solutions and investigated the temperature dependence of the monolayer ionic permeability. The higher ionic conductivity observed at high temperatures was interpreted in terms of structural changes in the film due to Ostwald ripening of the adsorbed thiol domains.

Given the ability of ionic species to permeate self-assembled monolayers in the presence of interfacial electric fields, the

(6) (a) Rampi, M. A.; Schueller, O. J. A.; Whitesides, G. M. *Appl. Phys. Lett.* **1998**, *72*, 1781. (b) Slowinski, K.; Fong, H. K. Y.; Majda, M. *J. Am. Chem. Soc.* **1999**, *121*, 7257. (c) Haag, R.; Rampi, M. A.; Holmlin, R. E.; Whitesides, G. M. *J. Am. Chem. Soc.* **1999**, *121*, 7895. (d) Slowinski, K.; Majda, M. *J. Electroanal. Chem.* **2000**, *491*, 139. (e) Holmlin, R. E.; Ismagilov, R. F.; Haag, R.; Mujica, V.; Rutner, M. A.; Rampi, M. A.; Whitesides, G. M. *Angew. Chem., Int. Ed.* **2001**, *40*, 2316. (f) Anariba, F.; McCreery, R. L. *J. Phys. Chem. B* **2002**, *106*, 10355. (g) Fan, F.-R. F.; Yang, J.; Cai, L.; Price, D. W.; Dirk, S. M.; Kosynkin, D. V.; Yao, Y.; Rawlett, A. M.; Tour, J. M.; Bard, A. J. *J. Am. Chem. Soc.* **2002**, *124*, 5550. (h) Rampi, M. A.; Whitesides, G. M. *Chem. Phys.* **2002**, *281*, 373. (i) York, R. L.; Nguyen, P. T.; Slowinski, K. *J. Am. Chem. Soc.* **2003**, *125*, 5948.

(7) (a) Miller, C.; Cuendet, P.; Grätzel, M. *J. Phys. Chem.* **1991**, *95*, 877. (b) Miller, C.; Grätzel, M. *J. Phys. Chem.* **1991**, *95*, 5225. (c) Becka, A. M.; Miller, C. J. *J. Phys. Chem.* **1992**, *96*, 2657. (d) Becka, A. M.; Miller, C. J. *J. Phys. Chem.* **1993**, *97*, 6233. (e) Terrettaz, S.; Becka, A. M.; Traub, M. J.; Fettinger, J. C.; Miller, C. J. *J. Phys. Chem.* **1995**, *99*, 11216.

(8) Xu, J.; Li, H.-L.; Zhang, Y. *J. Phys. Chem.* **1993**, *97*, 11497.

(9) Cheng, J.; Sàghi-Szabó, G.; Tossell, J. A.; Miller, C. J. *J. Am. Chem. Soc.* **1996**, *118*, 680.

(10) Napper, A. M.; Liu, H.; Waldeck, D. H. *J. Phys. Chem. B* **2001**, *105*, 7699.

(11) Sek, S.; Bilewicz, R. *J. Electroanal. Chem.* **2001**, *509*, 11.

(12) Slowinski, K.; Slowinska, K. U.; Majda, M. *J. Phys. Chem. B* **1999**, *103*, 8544.

(13) Demoz, A.; Harrison, D. J. *Langmuir* **1993**, *9*, 1046.

(14) Magnussen, O. M.; Ocko, B. M.; Deutsch, M.; Regan, M. J.; Pershan, P. S.; Abernathy, D.; Grüble, G.; Legrand, J.-F. *Nature* **1996**, *384*, 250.

(15) (a) Bruckner-Lea, C.; Janata, J.; Conroy, J.; Pungor, A.; Caldwell, K. *Langmuir* **1993**, *9*, 3612. (b) Bruckner-Lea, C.; Kimmel, R. J.; Janata, J.; Conroy, J. F. T.; Caldwell, K. *Electrochim. Acta* **1995**, *40*, 2897.

(16) (a) Slowinski, K.; Chamberlain, R. V.; Bilewicz, R.; Majda, M. *J. Am. Chem. Soc.* **1996**, *118*, 4709. (b) Slowinski, K.; Chamberlain, R. V.; Miller, C. J.; Majda, M. *J. Am. Chem. Soc.* **1997**, *119*, 11910.

(17) Calvente, J. J.; Andreu, R.; González, L.; Gil, M.-L. A.; Mozo, D.; Roldán, E. *J. Phys. Chem. B* **2001**, *105*, 5477.

(18) Yamamoto, H.; Waldeck, D. H. *J. Phys. Chem. B* **2002**, *106*, 7469.

(19) (a) Sek, S.; Misicka, A.; Bilewicz, R. *J. Phys. Chem. B* **2000**, *104*, 5399. (b) Sek, S.; Palys, B.; Bilewicz, R. *J. Phys. Chem. B* **2002**, *106*, 5907.

(20) Sumner, J. J.; Weber, K. S.; Hockett, L. A.; Creager, S. E. *J. Phys. Chem. B* **2000**, *104*, 7449.

(21) Porter, M. D.; Bright, T. B.; Allara, D. L.; Chidsey, C. E. D. *J. Am. Chem. Soc.* **1987**, *109*, 3559.

(22) (a) Boubour, E.; Lennox, R. B. *Langmuir* **2000**, *16*, 4222. (b) Boubour, E.; Lennox, R. B. *J. Phys. Chem. B* **2000**, *104*, 9004. (c) Boubour, E.; Lennox, R. B. *Langmuir* **2000**, *16*, 7464.

(23) Protsailo, L. V.; Fawcett, W. R. *Langmuir* **2002**, *18*, 8933.

following question arises whenever a freely diffusing redox species faces a SAM-coated electrode: Do ion permeation and long-range electron transfer across the monolayer occur on the same time scale or on different time scales such that they can be decoupled by using an appropriate transient technique? A related crucial point is whether ion permeation involves just a disordering of the adsorbed thiol structure or an irreversible breakdown of the monolayer, including desorption of some of its molecules. It is the aim of the present work to provide some new insights into these aspects via the study of the electroreduction of $Ru(NH_3)_6^{3+}$ at a series of carboxylic acid- and hydroxyl-terminated self-assembled monolayers deposited on mercury drop electrodes, by combining results obtained with distinct electrochemical techniques that give access to processes occurring at different time scales. Short and intermediate chain length hydroxyalkanethiols were chosen because they are more prone to undergo ion permeation within the available potential window. The use of mercaptoundecanoic acid is envisaged to produce less organized monolayers, at least in its outermost part, due to the presence of the bulkier −COOH terminal group. As a result, two types of electrochemical response have been observed, including (a) monolayers that preserve their tunneling barrier properties within the entire potential window prior to their reductive desorption and (b) monolayers exhibiting a potential-induced breakdown of their blocking properties, which is associated with the disordering and partial desorption of the film. Apart from its implications for long-range electron transfer processes at modified electrodes, the present results are also useful in understanding the factors that contribute to the electrical breakdown of self-assembled monolayers.

Experimental Section

Reagents. 4-Mercaptophenol (MPH), 6-mercapto-1-hexanol (MHOL), 11-mercapto-1-undecanol (MUOL), 11-mercaptoundecanoic acid (MUA), and $Ru(NH_3)_6Cl_3$ were purchased from Aldrich. 4-Mercapto-1-butanol (MBOL), sodium dihydrogen phosphate (NaH_2PO_4), and sodium hydroxide (NaOH) were purchased from Fluka Chemicals and used as received. Aqueous solutions were prepared from water purified with a Millipore Milli-Q system (resistivity 18 MΩ cm). Working solutions of thiols in sodium phosphate buffer were prepared from 5 mM stock solutions of MBOL and MHOL in water, and MPH, MUOL, and MUA in ethanol (Merck). These solutions were prepared daily and intensively deaerated with a presaturated nitrogen stream for at least 2 h prior to the measurements. Mercury was distilled three times under vacuum after treatment with dilute nitric acid and mercurous nitrate.

Self-Assembly of Thiols at Mercury. Short hydroxyalkanethiols are known to form soluble mercuric-thiolate compounds when they are brought in contact with mercury, unless the electrode is sufficiently polarized at negative overpotentials.[24,25] To avoid partial solubilization of ex situ formed thiol monolayers during the rinsing stage, in the present study SAMs were built up in situ under potentiostatic control, by holding the hanging mercury drop electrode (HMDE) at −0.05 V (versus Ag/AgCl, saturated NaCl) for ca. 60−100 s in the presence of a 100 μM thiol solution in sodium phosphate buffer, which may also contain the redox probe. The use of a low thiol concentration solution ensures that dissolved thiol molecules do not interfere with the electrochemical signal measured after the deposition step.

Electrochemical Measurements. Electrochemical measurements were carried out in a water-jacketed glass cell, thermostated at 25 ± 0.2 °C with a Haake D8.G circulator thermostat. A sodium-saturated Ag/AgCl electrode and a platinum foil were used as reference and auxiliary electrodes, respectively. The working electrode was an HMDE (EG&G PAR 303A) whose area (0.0275 cm^2) was determined by weighing three sets of 10 drops. Voltammetric, chronoamperometric, and cell impedance measurements were carried out with an Autolab/PGSTAT30 (Eco Chemie B. V.), equipped with a frequency response analyzer module.

Computational Aspects. Hartree−Fock calculations at the 3-21G basis set level were performed by using HyperChem to compute the molecular geometry of the studied organothiols. The molecular lengths were calculated as the distance between the sulfur atom and the hydrogen atom of either the hydroxyl or carboxylic terminal group. Then, a value of 2 Å was added to account for the distance between the sulfur atom of the thiol and the substrate.[18,26]

Results and Discussion

(a) In Situ Formation and Desorption of Thiol Self-Assembled Monolayers. To explore the influence of the thickness and chemical composition of the intervening medium on the electron transfer rate between mercury and $Ru(NH_3)_6^{3+}$, five thiol monolayers were studied. Figure 1 summarizes the voltammetric features of the in situ formed SAMs of MBOL, MHOL, MUOL, MUA, and MPH. In these experiments, the potential was first held at −0.05 V for a fixed period (60−100 s), after which it was swept toward more negative potentials to induce the reductive desorption of the previously formed monolayer. The insets show typical chronoamperograms recorded while thiol deposition was taking place at −0.05 V. Zero time in these chronoamperograms corresponds to the time at which the potential was stepped from −1.2 to −0.05 V in a double potential step experiment designed to remove any residual thiol adsorbed during formation of the mercury drop. The amount of adsorbed molecules in each monolayer was estimated from the area under the cathodic voltammetric wave, by assuming the exchange of one electron per thiol moiety. A value of 7.5×10^{-10} mol cm^{-2} was found for MBOL, whereas values in the 9×10^{-10} to 1×10^{-9} mol cm^{-2} range were obtained for MHOL, MPH, MUOL, and MUA. Within the uncertainty of the nonfaradaic contribution to the measured current, these values are consistent with a perpendicular orientation of the oxidized thiol molecules in the adsorbed state.[16b,27]

The location and shape of the reductive desorption waves provide some insight into the compactness of the SAM. As previously observed for methyl-terminated thiols,[28,29] an increase of the alkyl chain length in the ω-hydroxyalkanethiol series results in a shift of the peak potential toward more negative values, indicating the formation of more stable adsorbed structures. Replacement of the terminal −OH group by the bulkier −COOH group, which is either fully or partially deprotonated at pH = 7,[30−38] decreases the electrochemical stability of the monolayer, as evidenced by the fact that MUA

(24) Casassas, E.; Ariño, C.; Esteban, M.; Müller, C. *Anal. Chim. Acta* **1988**, *206*, 65.
(25) Gil, M.-L. A.; Andreu, R.; Calvente, J. J.; Pablos, F. *J. Electrochem. Soc.* **2002**, *149*, E45.
(26) Smalley, J. F.; Feldberg, S. W.; Chidsey, C. E. D.; Linford, M. R.; Newton, M. D.; Liu, Y.-P. *J. Phys. Chem.* **1995**, *99*, 13141.
(27) Muskal, N.; Turyan, I.; Mandler, D. *J. Electroanal. Chem.* **1996**, *409*, 131.
(28) Widrig, C. A.; Chung, C.; Porter, M. D. *J. Electroanal. Chem.* **1991**, *310*, 335.
(29) Stevenson, K. J.; Mitchell, M.; White, H. S. *J. Phys. Chem. B* **1998**, *102*, 1235.
(30) Lee, T. R.; Carey, R. I.; Biebuyck, H. A.; Whitesides, G. M. *Langmuir* **1994**, *10*, 741.
(31) Creager, S. E.; Clarke, J. *Langmuir* **1994**, *10*, 3675.
(32) White, H. S.; Peterson, J. D.; Cui, Q.; Stevenson, K. J. *J. Phys. Chem. B* **1998**, *102*, 2930.

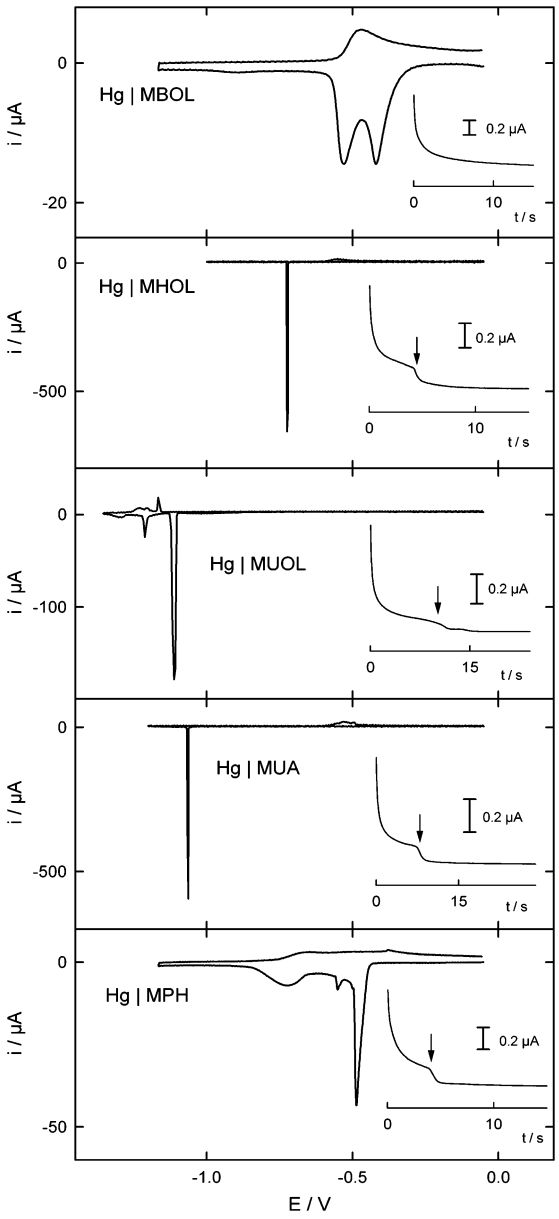

Figure 1. Cathodic stripping voltammograms recorded in solutions containing 100 μM indicated thiol and 0.25 M H_3PO_4, pH 7. Scan rate υ = 1 V s^{-1}, deposition potential $E_d = -0.05$ V, and deposition time 100 s. Insets show chronoamperograms recorded during the deposition step, as explained in the text.

desorbs at more positive potentials than MUOL. On the other hand, the replacement of the alkyl chain by a phenyl moiety of similar molecular length leads to a slightly more stable SAM for MPH, as compared to MBOL. In all cases, except for MBOL, voltammetric spikes with a full width at half-maximum less than 25 mV were obtained, which are indicative of strong lateral interactions between the adsorbed molecules.[39,40] The presence of voltammetric spikes in the cathodic scan correlates with the occurrence of a sudden decrease in the chronoamperometric current recorded during the deposition stage, which is not observed for MBOL (see arrows in the insets of Figure 1), which signals passivation of the mercury surface by the adsorbed thiol.

Either single or multiple desorption waves are recorded, which according to previous studies[17,29] can be attributed to distinct orientational states of the adsorbed molecules differing in their surface density. Conversion of a fraction of molecules from the higher to the lower surface density states is expected during the desorption of a densely packed monolayer, due to the free space that is continuously being created as molecules leave the electrode surface. The possibility of observing individual waves for each population depends on their relative stability. If the low surface density state is the most stable, it will require a more negative potential for its desorption. Under these conditions, at least two voltammetric waves are expected, as observed for MBOL and MPH. On the other hand, if the high surface density state is the most stable, adsorbed molecules in the low surface density state will be desorbed as soon as they are formed. In this last case, a single narrow voltammetric wave is expected, as observed for MHOL, MUOL, and MUA. The presence of small voltammetric peaks beyond the main reductive wave of MUOL suggests that a residual amount of reduced thiol molecules remains physisorbed on the electrode, and surface phase transitions involving these physisorbed molecules are likely to be the origin of these additional voltammetric features. Therefore, upon increasing the alkyl chain length, not only does the monolayer become more compact but the adsorption of the reduced thiol molecules is also promoted.[41]

(b) Comparison between $Ru(NH_3)_6^{3+}$ Electroreduction at Bare and Thiol-Coated Mercury Electrodes. Figure 2 shows how the heterogeneous electron transfer between Hg and $Ru(NH_3)_6^{3+}$ is affected by the presence of the SAMs indicated above. The voltammetric response corresponding to a bare mercury electrode has also been included for comparison. In the absence of any organic monolayer, the expected reversible wave for a fast monoelectronic charge transfer[42] (with a peak potential separation of ca. 60 mV) is only observed for low concentrations of the ruthenium complex ($\leq$1 mM). At higher concentrations, however, the cathodic peak current exceeds the value expected for a diffusion-controlled process, and the wave approaches the Gaussian-like shape typical of a surface-confined process. Under these conditions, the frequency dependence of the electrode admittance also confirms the presence of specifically adsorbed $Ru(NH_3)_6^{3+}$. It should be noted that adsorption of this redox couple on gold has recently been detected by laser-induced temperature jump experiments.[43] Any voltammetric indication of ruthenium adsorption disappears when the electrode is coated with a thiol monolayer, which now renders the overall appearance of voltammograms independent of ruthenium bulk concentration (see Figure 2).

(33) (a) Shimazu, K.; Teranishi, T.; Sugihara, K.; Uosaki, K. *Chem. Lett.* **1998**, *7*, 669. (b) Sugihara, K.; Teranishi, T.; Shimazu, K.; Uosaki, K. *Electrochemistry* **1999**, *67*, 1172.
(34) Smalley, J. F.; Chalfant, K.; Feldberg, S. W.; Nahir, T. M.; Bowden, E. F. *J. Phys. Chem. B* **1999**, *103*, 1676.
(35) Kakiuchi, T.; Iida, M.; Imabayashi, S.; Niki, K. *Langmuir* **2000**, *16*, 5397.
(36) Dai, Z.; Ju, H. *Phys. Chem. Chem. Phys.* **2001**, *3*, 3769.
(37) (a) Zheng, W.; Maye, M. M.; Leibowitz, F. L.; Zhong, C.-J. *Anal. Chem.* **2000**, *72*, 2190. (b) Luo, J.; Kariuki, N.; Han, L.; Maye, M. M.; Moussa, L. W.; Kowaleski, S. R.; Kirk, F. L.; Hepel, M.; Zhong, C.-J. *J. Phys. Chem. B* **2002**, *106*, 9313.
(38) (a) Schweiss, R.; Welzel, P. B.; Werner, C.; Knoll, W. *Langmuir* **2001**, *17*, 4304. (b) Schweiss, R.; Pleul, D.; Simon, F.; Janke, A.; Welzel, P. B.; Voit, B.; Knoll, W.; Werner, C. *J. Phys. Chem. B* **2004**, *108*, 2910.
(39) Laviron, E. *J. Electroanal. Chem.* **1979**, *100*, 263.
(40) Aoki, K.; Kakiuchi, T. *J. Electroanal. Chem.* **1998**, *452*, 187.
(41) Calvente, J. J.; Andreu, R.; Gil, M.-L. A.; Gonzalez, L.; Alcudia, A.; Domínguez, M. *J. Electroanal. Chem.* **2000**, *482*, 18.
(42) Bard, A. J.; Faulkner, L. R. *Electrochemical Methods: Fundamentals and Applications*; John Wiley & Sons: New York, 2001.
(43) Smalley, J. F.; Geng, L.; Chen, A.; Feldberg, S. W.; Lewis, N. S.; Cali, G. *J. Electroanal. Chem.* **2003**, *549*, 13.

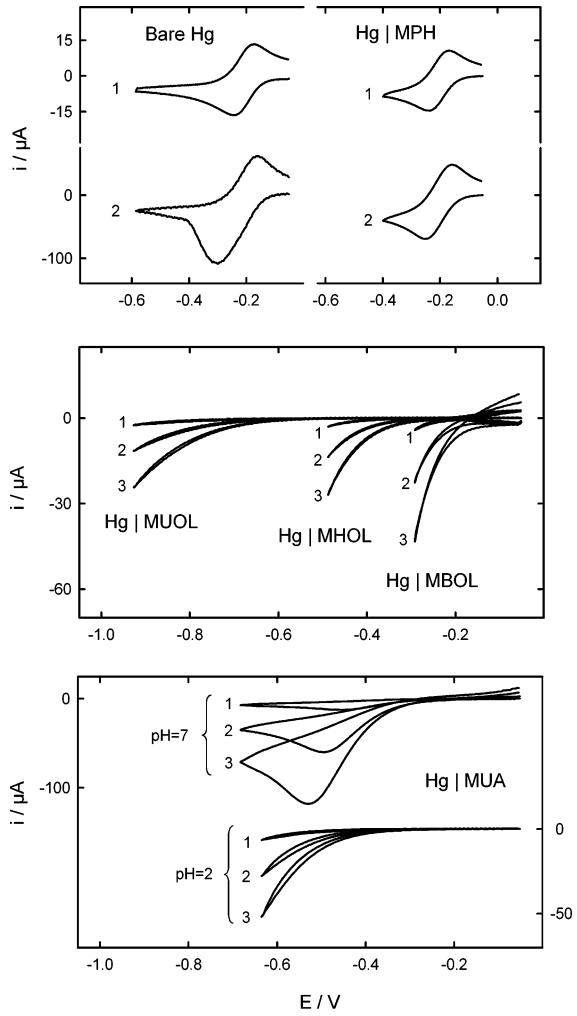

Figure 2. Cathodic stripping voltammograms recorded in solutions containing 100 μM corresponding thiol, 0.25 M H_3PO_4, pH 7, except for pH 2 solutions in the lowest panel, and (1) 1 mM $Ru(NH_3)_6^{3+}$, (2) 5 mM $Ru(NH_3)_6^{3+}$ and (3) 10 mM $Ru(NH_3)_6^{3+}$ at the HMDE. Scan rate $\upsilon = 1$ V s^{-1}, deposition potential $E_d = -0.05$ V, and deposition time 100 s. The nature of the thiol monolayer, if present, is indicated on each panel.

The specific influence of each monolayer on the rate of electron transfer is determined by the chain length and chemical composition of the adsorbed thiol. Two limiting cases can be identified. First, reversible voltammetric waves were obtained at MPH-coated electrodes, providing evidence for a rather fast electron transfer between Hg and $Ru(NH_3)_6^{3+}$. At the opposite extreme, exponential-like voltammograms were obtained at hydroxyalkanethiol-coated electrodes, which are typical of a redox process limited by a slow rate of electron transfer across the monolayer. Upon increasing the alkyl chain length of the thiol, reduction currents appear at progressively more negative potentials, indicating a slower electron transfer rate at a given overpotential. This behavior is to be expected when $Ru(NH_3)_6^{3+}$ remains on the solution side of the monolayer, so that an increase of the monolayer thickness results in the activation plane for electron transfer being moved away from the electrode surface. The same increase in the thiol chain length also produces an obvious decrease of the current versus potential slopes, which reflects the gradual leveling off of the activation-energy/driving-force relationship as the overpotential increases, as predicted by Marcus DOS theory.[42,44] The high degree of reproducibility of the voltammetric features (typically within 2%) strongly supports the assumption of monolayers being defect-free, since larger dispersions are to be expected in the presence of a random fraction of pinholes and defects.[4]

Between these two limiting situations, MUA-coated mercury electrodes exhibit intermediate behavior, characterized by peaked voltammograms located at large negative overpotentials, which are typical of mixed activation/diffusion control. On the other hand, the enhancement of the current, as compared to voltammograms obtained in the presence of other thiols with a similar hydrocarbon chain length such as MUOL, indicates that some partitioning of the $Ru(NH_3)_6^{3+}$ species into the monolayer may occur, thus allowing for a closer approach of the redox probe to the mercury surface. Since the adsorbed MUA is either fully or partially deprotonated at pH 7 (reported pK_a values are within the range 4.4−10.3[30−38]), ionic partitioning is likely to be related to the presence of the negatively charged carboxylate groups. To further explore this point, additional experiments were carried out at pH 2, where carboxylic groups are expected to remain in their neutral form. As shown in the lower panel of Figure 2, protonation of the carboxylate group results in exponential-like voltammograms, resembling those obtained with hydroxy-terminated SAMs. This result is consistent with the pH dependence reported for this redox probe at MUA-modified gold electrodes.[4]

Before attempting a more detailed analysis of the electron transfer rate, we shall take advantage of the high sensitivity of the tunneling current to the distance of closest approach of $Ru(NH_3)_6^{3+}$ to the electrode (as illustrated in Figure 2 for the series of hydroxy-terminated SAMs), to explore the electrochemical stability of these monolayers on an expanded time scale.

(c) Potential-Induced Gating of Self-Assembled Monolayers. Recent reports by Boubour and Lennox[22] have demonstrated that below a critical potential a variety of SAMs deposited on gold lose their barrier properties against ion permeation. This observation, which is relevant in relation to the stability of interfacial structures and to studies of long-range electron transfer, raises the issue of the extent to which the compactness of the monolayer is preserved on the time scale of a voltammetric experiment. To explore whether the apparent absence of $Ru(NH_3)_6^{3+}$ permeation across OH-terminated SAMs is governed by either thermodynamic or kinetic restrictions, a chronoamperometric protocol has been adopted. In this way, the barrier properties of these monolayers against ion permeation can be checked over an extended time scale at a fixed applied potential. To detect any disruption of the monolayer, the use of the soluble redox probe allows us to take advantage of the exponential dependence of the electron transfer rate on the donor−acceptor distance,[45] so that an increase of the current is expected whenever $Ru(NH_3)_6^{3+}$ permeates the monolayer.

Figure 3 shows a series of chronoamperograms corresponding to $Ru(NH_3)_6^{3+}$ reduction at ω-hydroxyalkanethiol-coated mercury electrodes. These were recorded after stepping the potential from the deposition potential (E_d) to a more negative potential value (E_{fin}), located within the capacitive range depicted in

(44) Schmickler, W. *Interfacial Electrochemistry*; Oxford University Press: New York, 1996.
(45) Barbara, P. F.; Meyer, T. J.; Ratner, M. A. *J. Phys. Chem.* **1996**, *100*, 13148.

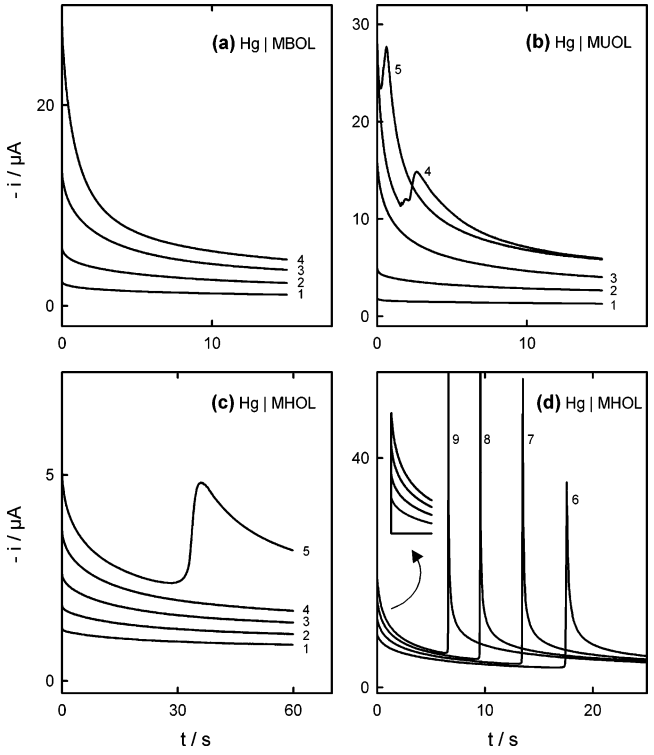

Figure 3. Chronoamperograms recorded at (a) MBOL-, (b) MUOL-, and (c,d) MHOL-coated mercury electrodes in solutions containing 5 mM $Ru(NH_3)_6^{3+}$, 100 μM indicated thiol, and 0.25 M H_3PO_4, pH 7, as a function of the final pulse potential E_{fin}: (1) −0.20, (2) −0.24, (3) −0.28, and (4) −0.32 V for MBOL; (1) −0.74, (2) −0.84, (3) −1.0, (4) −1.07, and (5) −1.12 V for MUOL; (1) −0.34, (2) −0.36, (3) −0.38, (4) −0.40, (5) −0.42, (6) −0.46, (7) −0.48, (8) −0.50, and (9) −0.52 V for MHOL. The monolayers were formed under potentiostatic control at $E_d = -0.05$ V with a deposition time of 100 s. The inset in panel (d) shows a magnification of the initial current decays.

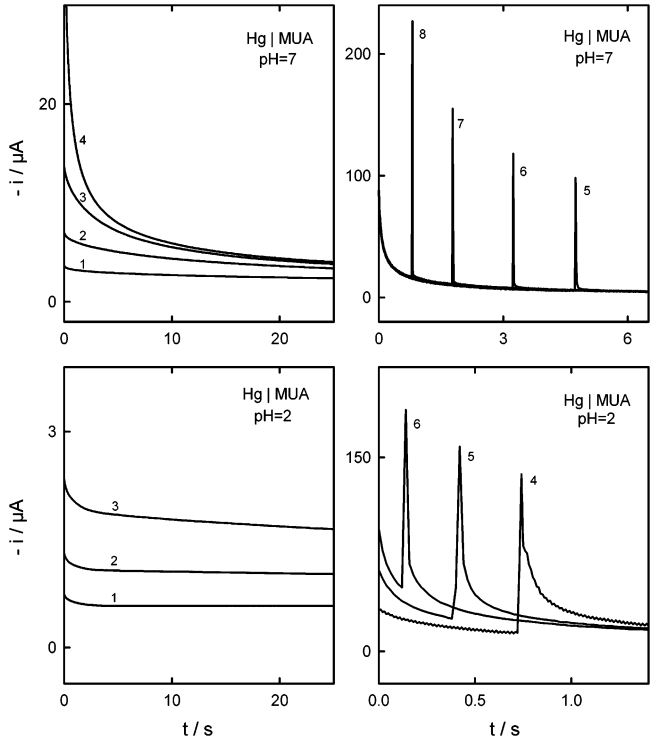

Figure 4. Chronoamperograms recorded at MUA-coated mercury electrodes in solutions containing 5 mM $Ru(NH_3)_6^{3+}$, 100 μM MUA, 0.25 M H_3PO_4 at pH 7 and pH 2, as a function of the final pulse potential E_{fin}: (1) −0.28, (2) −0.32, (3) −0.36, (4) −0.44, (5) −0.58, (6) −0.60, (7) −0.62, and (8) −0.70 V for the pH 7 solution, and (1) −0.36, (2) −0.40, (3) −0.44, (4) −0.64, (5) −0.72, and (6) −0.84 V for the pH 2 solution. The monolayer was formed under potentiostatic control at $E_d = -0.05$ V with a deposition time of 100 s.

Figure 1 (i.e., before the onset of the thiol desorption waves). Some striking differences were observed within this series of SAMs that differ in their chain length. Mercury electrodes coated with MBOL exhibited monotonically decreasing transients (Figure 3). As anticipated on the basis of its voltammetric features in Figure 2, these chronoamperometric profiles are consistent with a kinetically controlled redox process, indicating that at these potentials the monolayer preserves its electronic barrier properties over a prolonged period (at least up to ∼60 s). Analogous behavior was observed in the presence of MPH monolayers (not shown), where a set of smooth diffusion-controlled transients were recorded within the available potential window, as expected for a fast redox process.

On the other hand, we have observed that current peaks occur spontaneously along the transients recorded from MUOL- and MHOL-coated electrodes (Figure 3b−d). These peaks appear only when the potential is made more negative than a critical value (i.e., when $E_{fin} \leq E_{crit}$, with $E_{crit} = -0.43 \pm 0.02$ V or $E_{crit} = -0.98 \pm 0.03$ V, in the case of MHOL and MUOL monolayers, respectively), and they become narrower and shift toward shorter times as E_{fin} is made progressively more negative. Before the onset of the chronoamperometric peak (i.e., for $t < t_{max}$), the current profile depends on the applied potential, indicating that it is controlled by electron transfer kinetics (see inset in Figure 3d). However, beyond the peak (i.e., for $t > t_{max}$), the current decay becomes insensitive to the applied potential, signaling that it is controlled by mass transport of the redox probe (Cottrellian behavior). Therefore, the post-peak increase of the reduction rate indicates that the occurrence of the chronoamperometric peak can be attributed to a sudden permeation of the monolayer by $Ru(NH_3)_6^{3+}$. As with the voltammetric features, the current prior to the chronoamperometric peak was highly reproducible. However, it should be noted that the precise location of the peak (t_{max}) shows some scatter (up to 20% in the vicinity of the critical potential), which becomes smaller as the potential is made more negative. This suggests that the monolayer breakdown at potentials close to E_{crit} is initiated at transient defects produced by thermal fluctuations in the lateral structure of the thiol monolayer.[46]

Reduction of $Ru(NH_3)_6^{3+}$ at MUA-coated electrodes also generates peaked chronoamperograms, though their characteristics are somewhat dependent on the solution pH (Figure 4). At pH 2, the chronoamperometric features are similar to those obtained from MHOL-coated electrodes, showing the transition from a kinetically controlled current, prior to the appearance of the peak, to a diffusion-limited current beyond the peak. However, the current peaks become extremely narrow at pH 7 and, interestingly, they emerge from a diffusion-controlled transient, which exhibits Cottrellian behavior before and after the current peak. This latter observation suggests that at pH 7 the redox probe can easily permeate the outer part of the MUA monolayer and that chronoamperometric spikes may originate from a disordering of the innermost part of the monolayer.

(46) Bordi, F.; Cametti, C.; Motta, A. *J. Phys. Chem. B* **2000**, *104*, 5318.

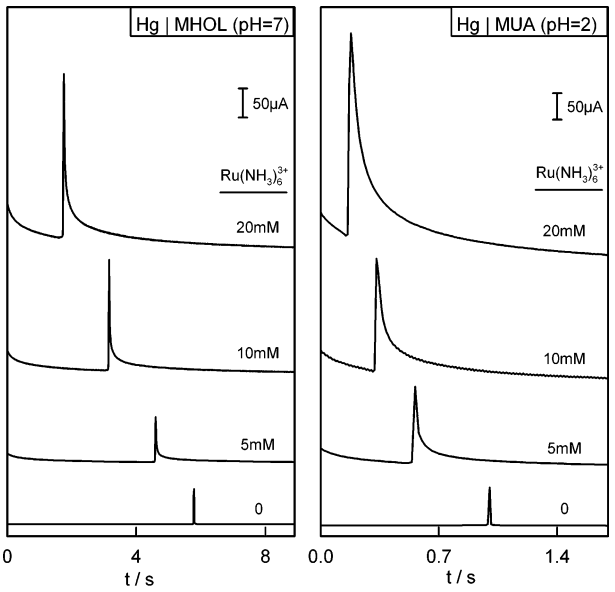

Figure 5. Influence of $Ru(NH_3)_6^{3+}$ concentration on chronoamperograms recorded at MHOL- and MUA-coated mercury electrodes in solutions containing the indicated concentrations of $Ru(NH_3)_6^{3+}$, 100 μM corresponding thiol, 0.25 M H_3PO_4 at pH 7 (for MHOL) and pH 2 (for MUA). Monolayers were formed under potentiostatic control at $E_d = -0.05$ V with a deposition time of 100 s. The final pulse potentials are $E_{fin} = -0.520$ V and $E_{fin} = -0.680$ V for MHOL and MUA monolayers, respectively. For the sake of clarity, chronoamperograms have been shifted vertically.

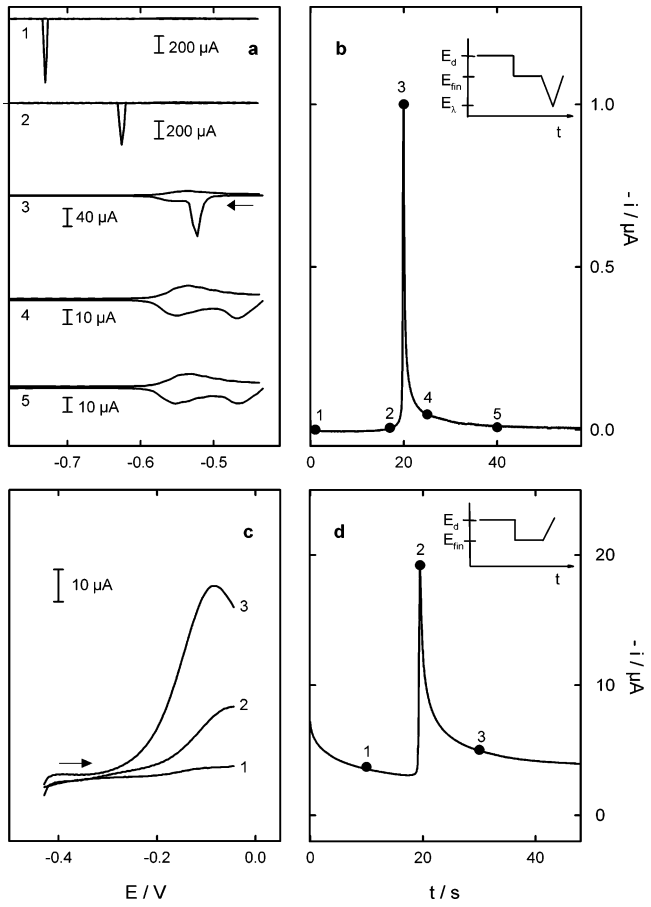

Figure 6. (a) Reductive desorption voltammograms for a MHOL-coated Hg electrode recorded at the times indicated along the chronoamperometric curve in (b), by using the potential program depicted in the inset with $E_d = -0.05$ V, $E_{fin} = -0.44$ V, and $E_\lambda = -1.0$ V. Deposition time 100 s, scan rate $\upsilon = 1.0$ V s^{-1}, and solution composition: 100 μM MHOL in 0.25 M H_3PO_4, pH 7 buffer. (c) Voltammograms corresponding to the reoxidation of generated $Ru(NH_3)_6^{2+}$ at $E_{fin} = -0.44$ V on a MHOL-coated Hg electrode, recorded at the times indicated along the chronoamperometric curve in (d) by using the potential program depicted in the inset with $E_d = -0.05$ V, $E_{fin} = -0.44$ V. Deposition time $t_d = 100$ s, scan rate $\upsilon = 1$ V s^{-1}, and solution composition: 5 mM $Ru(NH_3)_6^{3+}$ and 100 μM MHOL in 0.25 M H_3PO_4 pH 7 buffer.

It should be noted that these chronoamperometric spikes are also observed in the absence of $Ru(NH_3)_6^{3+}$. Figure 5 shows how successive additions of the redox probe result in increased current transients, which are progressively shifted toward shorter times. The current increase nicely demonstrates the amplification effect of the redox probe, though it is also evident that it is far from behaving like a passive probe. The presence of $Ru(NH_3)_6^{3+}$ helps to break down the barrier properties of the thiol monolayer in the presence of an external electric field, and its disruptive action increases with concentration. This finding corroborates the expectation that the delay time for the monolayer breakdown is governed by the rate of ion permeation, and it also suggests that electrostatic effects play an important role due to the more rapid incorporation of the triply charged $Ru(NH_3)_6^{3+}$ compared to that of the monovalent Na^+ cation of the buffer solution.

Additional insight into the dynamic behavior of these monolayers was gained by recording fast scan voltammograms at certain intervals along the chronoamperograms. These voltammograms were obtained either in the absence or in the presence of $Ru(NH_3)_6^{3+}$, and two complementary protocols, whose potential programs are depicted in the insets of Figure 6, were followed. First, the MHOL monolayer was formed in the absence of $Ru(NH_3)_6^{3+}$, and the previous double step chronoamperometric experiments were again observed to produce peaked current transients. The intensity of the current transients, which must now be related to a rearrangement of the interfacial structure, is obviously much lower (Figure 6b). Reductive desorption voltammograms were recorded at five characteristic times along the chronoamperogram. When the potential was held at E_{fin} for a time less than t_{max}, single desorption waves were obtained whose peak potential shifts to more positive values as the dwell time at E_{fin} increases (voltammograms 1 and 2 in the upper panels of Figure 6). Since the number of adsorbed MHOL molecules determined from the areas under these voltammograms remains constant, this result indicates that a progressive disordering of the monolayer is taking place for $t < t_{max}$. When the dwell time approaches or exceeds t_{max}, a significant desorption of thiol takes place. For instance, the area under voltammograms 4 and 5 in Figure 6a implies a loss of half of the thiols from the monolayer ($\Delta\Gamma_{MHOL} \approx -5 \times 10^{-10}$ mol cm^{-2}). Their voltammetric features are in agreement with the behavior to be expected of a poorly structured mixture of adsorbates, where a less stable population of closely packed thiol molecules coexists with a more stable population of thiol molecules at low surface density.[17] It should be noted that the extent of MHOL desorption accompanying the chronoamperometric peak increases as the potential is made more negative, and that for $E_{fin} < -0.6$ V full desorption occurs.

In the second protocol (Figure 6c,d), the monolayer was deposited in the presence of $Ru(NH_3)_6^{3+}$, and its inhibitive barrier properties against the reoxidation of electrochemically generated $Ru(NH_3)_6^{2+}$ were tested by scanning the potential toward more positive values. The transition from a nearly flat

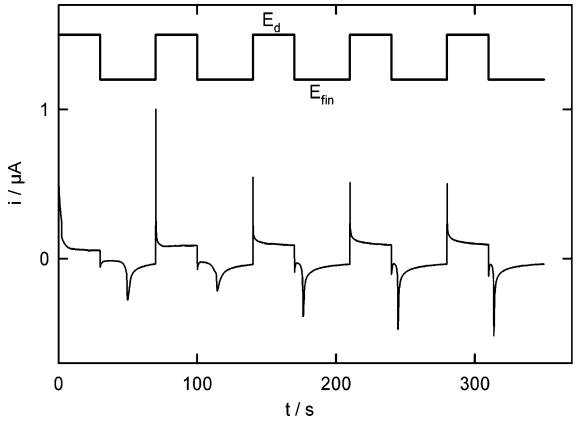

Figure 7. Transient response of a Hg electrode to the square waveform potential depicted in the upper plot. Deposition and final potentials are $E_d = -0.05$ V and $E_{fin} = -0.44$ V, respectively. Solution composition: 100 μM MHOL in 0.25 M H_3PO_4, pH 7 buffer.

voltammogram (curve 1 in Figure 6c), obtained for a time shorter than t_{max}, to a peaked voltammogram (curve 3 in Figure 6c), obtained for a time longer than t_{max}, also points to a partial desorption of the SAM at the chronoamperometric maximum.

The reversibility of this potential-induced rearrangement in the monolayer was checked by applying a cyclic square wave potential perturbation to the electrode, so that the potential was switched between the deposition potential and a second potential where the monolayer partially desorbs. The results obtained for a deposition potential of -0.05 V and a disordering potential of -0.44 V are shown in Figure 7. The appearance of the chronoamperometric peak in the successive disordering potential steps demonstrates the reversibility of the adsorption/desorption process. However, it should be noted that the current peak after each disordering pulse, associated with partial desorption, shifts to shorter times as compared to the preceding one, indicating that the monolayer gradually loses its ability to restore the original compactness at the deposition potential.

(d) Determination of Electron Transfer Rate Constants. As is clear from Figure 2, $Ru(NH_3)_6^{3+}$ reduction rates at bare and MPH-coated mercury electrodes are much higher than at electrodes modified with ω-functionalized alkanethiol monolayers. In these two cases, electron transfer rate constants were obtained from faradaic impedance measurements,[47,48] whereas large amplitude dc techniques were found to be more appropriate to determine the lower rate constant values that are characteristic of mercury electrodes modified with MBOL, MHOL, MUOL, and MUA monolayers. A detailed analysis of the electrode admittance to derive electron transfer rate constants at bare and MPH-modified mercury electrodes is reported elsewhere.[48]

Two alternative approaches have been used to determine the electron transfer rate constants at ω-functionalized alkanethiol-coated Hg electrodes: (i) analysis of the chronoamperometric response at short times and (ii) convolution voltammetry.

For a simple redox process:

$$O + ne^- \underset{k_b}{\overset{k_f}{\rightleftharpoons}} R \qquad (1)$$

the chronoamperometric response to a potential step from a

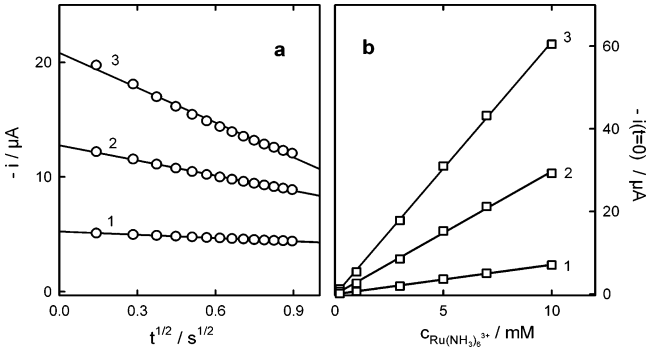

Figure 8. (a) Linear analysis of the transient response of a 5 mM $Ru(NH_3)_6^{3+}$, 100 μM MHOL, 0.25 M H_3PO_4, pH 7 solution for several values of the final pulse potential E_{fin}: (1) -0.42, (2) -0.48, (3) -0.52 V on a MHOL-coated Hg electrode. (b) Dependence of the linear analysis intercepts in (a) on $Ru(NH_3)_6^{3+}$ bulk concentration for the following final pulse potentials E_{fin}: (1) -0.40, (2) -0.50, (3) -0.56 V. The MHOL self-assembled monolayer was formed under potentiostatic control at $E_d = -0.05$ V during 100 s.

value outside to a value inside the faradaic region is given by:[49]

$$i(t) = -nFAk_f c_O^* \left[\left(1 - \frac{D^{1/2}}{Zr_o} \right) \exp(Z^2 t) \mathrm{erfc}(Zt^{1/2}) + \frac{D^{1/2}}{Zr_o} \right] \qquad (2)$$

where erfc stands for the complement of the error function, D is the diffusion coefficient of either O or R, which are assumed to take the same value, r_o is the electrode radius, c_O^* is the bulk concentration of the oxidized form, and Z is defined as:

$$Z = \frac{k_f + k_b}{D^{1/2}} + \frac{D^{1/2}}{r_o} \qquad (3)$$

At sufficiently short times, eq 2 reduces to:

$$i(t) = -nFAk_f c_O^* \left[1 - \frac{2(k_f + k_b)t^{1/2}}{(\pi D)^{1/2}} \right] \qquad (4)$$

According to this last expression, k_f can be evaluated from the intercept of a linear i versus $t^{1/2}$ plot. The applicability of this simplified procedure depends on the magnitude of $k_f + k_b$, since the higher the value of $k_f + k_b$, the narrower the time interval will be over which such a linear dependence can be observed. More reliable values of k_f can be determined when the intercepts obtained in the presence of several reactant concentrations are compared. Figure 8 illustrates this type of analysis in the case of $Ru(NH_3)_6^{3+}$ reduction at a MHOL-coated Hg electrode. Often, the linear part of the i versus $t^{1/2}$ plots extends up to ~0.8 s (Figure 8a). It is also observed that the intercepts increase linearly with ruthenium concentration (Figure 8b), thus confirming the adequacy of the first-order kinetic analysis, so that the slopes of the $i(t = 0)$ versus c_O^* plots provide the value of k_f at each potential.

The second approach makes use of convolution voltammetry[42,50,51] to calculate the concentrations of the electroactive

(47) Protsailo, L. V.; Fawcett, W. R. *Electrochim. Acta* **2000**, *45*, 3497.
(48) Ramirez, P.; Andreu, R.; Calvente, J. J.; Calzado, C. J.; Lopez-Perez, G. *J. Electroanal. Chem.*, in press.
(49) MacDonald, D. D. *Transient Techniques in Electrochemistry*; Plenum Press: New York, 1977. It should be noted that in this reference the equivalents of eqs 2 and 4 (there eqs 4.115 and 4.116 on page 84) contain errors in the signs.
(50) Oldham, K. J. *Anal. Chem.* **1986**, *58*, 2296.
(51) Savéant, J. M. *J. Phys. Chem. B* **2002**, *106*, 9387.

species in the vicinity of the electrode surface, according to:

$$c_O^s = c_O^* + \frac{I}{nFAD^{1/2}} \quad (5)$$

$$c_R^s = \frac{-I}{nFAD^{1/2}} \quad (6)$$

where I stands for the convolution current, here calculated for spherical geometry,[50] and c_i^s is the concentration of the ith species at the electron transfer plane at any time during the voltammetric scan.

By substituting eqs 5 and 6 into the expression for the current:

$$i = nFA(k_b c_R^s - k_f c_O^s) \quad (7)$$

and taking into account that thermodynamics requires that $k_b/k_f = \exp[(nF/RT)(E - E_h^o)]$, the following expression for the logarithm of the cathodic rate constant is obtained:

$$\ln k_f = \ln \frac{iD^{1/2}}{I_L - I\left\{1 + \exp\left[\frac{nF}{RT}(E - E_h^o)\right]\right\}} \quad (8)$$

where $I_L = -nFAc_O^*D^{1/2}$ is the limiting value of I as $c_O^s \rightarrow 0$. Values of the diffusion coefficient $D = (5.0 \pm 0.3) \times 10^{-6}$ cm^2 s^{-1} and of the formal potential $E_h^o = -0.210 \pm 0.005$ V (at pH 7) and $E_h^o = -0.150 \pm 0.005$ V (at pH 2) were determined from the convolution analysis of 1 mM $Ru(NH_3)_6^{3+}$ voltammograms obtained in the presence of the same supporting electrolyte at a bare mercury electrode. As a test of internal consistency, the same diffusion coefficient value was found from the Cottrell analysis of chronoamperograms recorded at $E = -0.6$ V (i.e., within the diffusion-limited potential region).

(e) Potential and Distance Dependence of the Electron Transfer Rate. Figure 9 summarizes the ln k_f values obtained for the reduction of $Ru(NH_3)_6^{3+}$ at the bare and thiol-coated mercury electrodes as described in the previous section. The good agreement between the two sets of results derived from chronoamperometry and convolutive voltammetry is illustrated in Figure 9a for MBOL, MHOL, MUOL, and MUA (at pH 2) monolayers. In general, kinetic parameters corresponding to intact thiol structures can be determined at more negative potentials by the chronoamperometric approach, since a premature breakdown of the monolayer occurs in voltammetric experiments during the potential scan. To asses the extent of double layer effects in the presence of ω-functionalized alkanethiol monolayers, experiments at MHOL-coated electrodes in a more concentrated buffer solution (1.0 M phosphate buffer, pH 7) were carried out. Although the formal standard potential shifts to a more negative value by ~ -30 mV, the dependence of ln k_f on overpotential coincides with that obtained in 0.25 M phosphate buffer solutions, demonstrating the absence of significant double layer effects.

As shown in Figure 9a, an increase of the spacer chain length in OH-terminated alkanethiol monolayers results in a decrease of both rate constant and apparent charge transfer coefficient values at a given potential. The first observation is a direct consequence of the increased distance between donor (electrode) and acceptor (ruthenium complex) centers, whereas the second

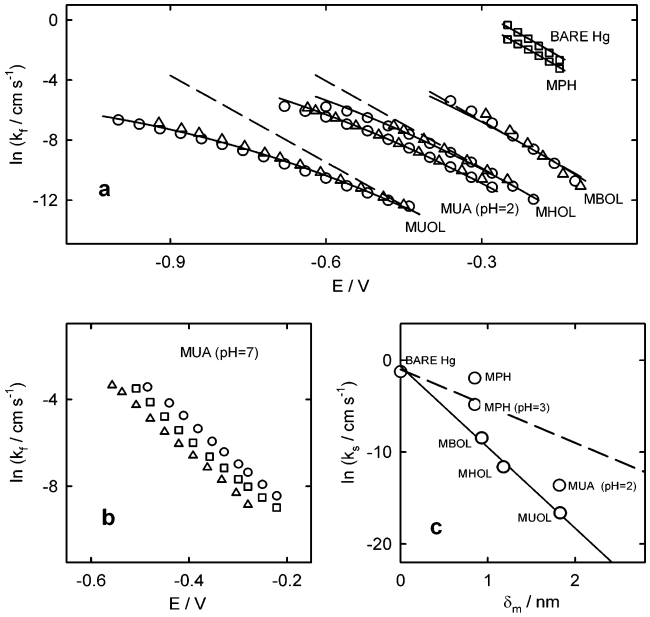

Figure 9. (a) Potential dependence of the heterogeneous electron transfer rate constant for the $Ru(NH_3)_6^{3+}$ electroreduction at the bare and the indicated SAM-coated Hg electrodes. Circles and triangles are experimental data derived from chronoamperometry and convolutive voltammetry, respectively. Squares are experimental data derived from electrode admittance analysis (ref 48). Solid lines represent the best fits to eq 9 with $\lambda = 1.05$ eV, whereas dashed lines represent the $\lambda \rightarrow \infty$ limit. (b) Dependence on $Ru(NH_3)_6^{3+}$ bulk concentration: (○) 1 mM, (□) 5 mM, and (△) 10 mM of the ln k_f vs E plots for the $Ru(NH_3)_6^{3+}$ electroreduction at a MUA-coated Hg electrode, as determined in a pH 7 buffer solution. (c) $Ru(NH_3)_6^{3+/2+}$ standard electron transfer rate constant (k_s) values obtained at different SAM-coated Hg electrodes, as a function of the theoretically estimated monolayer thickness δ_m. Solid line is the least-squares fit to the results corresponding to hydroxy-terminated alkanethiol monolayers. Broken line corresponds to a decay constant $\beta = 4$ nm^{-1}.

one is in agreement with Marcus' theory predictions, when the free energy difference between reactants and products approaches the value of the reorganization energy.

Within the framework of Marcus DOS theory, the potential dependence of k_f is given by:[5a,44,52]

$$k_f(\eta) = \frac{k_s}{Y_f}\int_{-\infty}^{+\infty} \frac{\exp\left[-\frac{(\xi_F - \xi + e_o\eta + \lambda)^2}{4\lambda kT}\right]}{1 + \exp\left(\frac{\xi - \xi_F}{kT}\right)} d\xi \quad (9)$$

where k is the Boltzmann constant, e_o is the electron charge, ξ is the energy of a given electronic state in the electrode, ξ_F is the energy of the Fermi level of the electrode (i.e., e_oE where E is the applied potential), η is the formal overpotential (i.e., the applied potential relative to the formal standard potential), λ is the medium reorganization energy, k_s is the standard rate constant, and Y_f represents the integral in eq 9 evaluated at $\eta = 0$.

Reorganization free energies are determined more accurately at high overvoltages. In our case, this situation corresponds to the reduction of $Ru(NH_3)_6^{3+}$ at MUOL-modified electrodes (see Figure 9a), which gives $\lambda = 1.05 \pm 0.05$ eV. This value was found to reproduce also the ln k_f versus E dependence obtained at the bare mercury electrode and in the presence of MPH,[48] MBOL, MHOL, and MUA (at pH 2) monolayers,

(52) Weber, K.; Creager, S. E. *Anal. Chem.* **1994**, *66*, 3164.

though the curvature of these last plots was less sensitive to the actual value of λ. Solid lines in Figure 9a are theoretical fits to eq 9 with $\lambda = 1.05$ eV, whereas dashed lines reproduce the $\lambda \rightarrow \infty$ limit of eq 9, which can be considered representative of the expected Butler−Volmer behavior with a charge transfer coefficient $\alpha = 0.5$. Even though both approaches reproduce the potential dependence of the electron transfer rate constants in the presence of the shortest thiol monolayer, only the Marcus' treatment is able to fit the data in the presence of the longer thiol monolayers, where higher overvoltages are needed to sustain the electron transfer process at a reasonable rate.

Quantitative agreement with Marcus DOS theory has also been reported before in relation to electron exchange of soluble redox probes at thiol-modified gold electrodes.[7] However, previous studies performed at modified mercury electrodes did not seem to support theoretical predictions to the same extent.[16b,53] In fact, a combination of concentration polarization effects, and a limited potential window, can easily obscure the curvature of the ln k_f versus E plots. It should be noted that upon neglecting the small mass transport effects in the analysis of the voltammetric curves that appear in Figure 2, linear ln k_f versus E relationships are obtained, with apparent charge transfer coefficient values that vary with the alkyl chain length: $\alpha = 0.5$, 0.4, and 0.25 for MBOL, MHOL, and MUOL monolayers, respectively.

The above estimate of the reorganization free energy is somewhat smaller than the value reported by Miller et al.[7c] (1.3−1.6 eV) for the electroreduction of $Ru(NH_3)_6^{3+}$ at ω-hydroxyalkanethiol-modified gold electrodes, but it is in good agreement with theoretical estimates from the inner sphere contribution $\lambda_{is} = 0.16$ eV, reported by Brown and Sutin,[54] and the outer sphere contribution λ_{os} computed from the three-phase electrostatic model of Liu and Newton:[55]

$$\lambda_{os} = \left(\frac{1}{\epsilon_I^{op}} - \frac{1}{\epsilon_I^{st}}\right)\frac{(\Delta e)^2}{2a} - \left(\frac{\theta_{II,I}^{op}}{\epsilon_I^{op}} - \frac{\theta_{II,I}^{st}}{\epsilon_I^{st}}\right)\frac{(\Delta e)^2}{4d} + \sum_{n=1}^{\infty}\left[\frac{\epsilon_{II}^{op}(\theta_{II,I}^{op})^{n-1}(\theta_{II,III}^{op})^n}{(\epsilon_{II}^{op} + \epsilon_I^{op})^2} - \frac{\epsilon_{II}^{st}(\theta_{II,I}^{st})^{n-1}(\theta_{II,III}^{st})^n}{(\epsilon_{II}^{st} + \epsilon_I^{st})^2}\right]\frac{(\Delta e)^2}{d + nL} \quad (10)$$

where

$$\theta_{i,j} = \frac{\epsilon_i - \epsilon_j}{\epsilon_i + \epsilon_j} \quad (11)$$

and subscripts I, II, and III refer to the aqueous solution, the film, and the electrode, respectively; superscripts op and st denote the optical and static values of the dielectric permittivity ϵ, respectively; L is the thickness of the film, a is the radius of the model spherical cavity containing the redox species, d is the distance from the redox species center to the film|solution interface, and Δe is charge exchanged in the redox process. The following parameter values were used to calculate λ_{os} with eq 10: $\Delta e = e_o$, $\epsilon_{III}^{st} = \epsilon_{III}^{op} = \infty$, $\epsilon_{II}^{op} = 2.25$,[55] $\epsilon_I^{st} = 78$, $\epsilon_I^{op} = 1.8$,[56] $d = a = 0.335$ nm,[57] $L = \delta_m$, where e_o is the electron charge,

Table 1. Measured Differential Capacitance (C_d), Theoretical Estimate of the Monolayer Thickness (δ_m), Relative Permittivity of the Monolayer (ϵ), outer-sphere Contribution to the Reorganization Energy Calculated from the Liu and Newton Model[55] and Standard Electron Transfer Rate Constant for the $Ru(NH_3)_6^{3+/2+}$ Redox Couple at the Thiol-Modified Mercury Electrodes Used in the Present Study

thiol monolayer	$C_d/\mu F\ cm^{-2}$	δ_m/nm	ϵ	$\lambda_{os,calc}$/eV	k_s/cm s^{-1}
MPH	7.2[a]	0.85[a]	6.9	0.93	0.13[a]
MBOL	11.	0.93	12.	0.95	2.1×10^{-4}
MHOL	3.6	1.18	4.8	0.96	9.0×10^{-6}
MUOL	1.9	1.83	3.9	1.00	6.0×10^{-8}
MUA (pH2)	2.1[b]	1.82	4.3	1.00	1.2×10^{-6}

[a] From ref 48. [b] The same value is obtained in acid and neutral pH solutions.

δ_m is a theoretical estimate of the monolayer thickness as described in the Computational Aspects, and $\epsilon_{II}^{st} = \epsilon$, where ϵ is the relative dielectric permittivity of the monolayer, which is determined from the measured differential capacitance values by assuming a simple capacitor model for the film and neglecting the small contribution from the diffuse layer:

$$\epsilon = \frac{C_d \delta_m}{\epsilon_o} \quad (12)$$

Values of δ_m, ϵ, and λ_{os} for the systems under study are summarized in Table 1, from which it can be seen that the experimental estimate of λ is close enough to the range (1.09−1.16) eV predicted for $\lambda_{is} + \lambda_{os}$.

A linear relationship between the logarithm of the standard rate constant k_s and the monolayer thickness δ_m was found (Table 1 and Figure 9c), in agreement with the well-known exponential decay of the electronic coupling factor with the donor−acceptor separation distance.[45] A decay constant β of 0.9 Å^{-1} (or 1.12 per methylene group) was estimated from the slope of the ln k_s versus δ_m plot for the ω-hydroxyalkanethiol monolayers. This estimate is in good agreement with previously reported values for thiol-modified mercury[16b] and gold electrodes[5f,7c,26,58] and with theoretical predictions for electron transfer processes taking place across alkanethiol molecular bridges.[59] From the intercept, a value of $k_s(\delta_m = 0) = 0.5$ cm s^{-1} was obtained, which is in excellent agreement with our own estimate (0.29 ± 0.05 cm s^{-1}) and with literature values (0.7 ± 0.2 cm s^{-1}),[60] (0.35 cm s^{-1}),[61] and (0.45 ± 0.12 cm s^{-1}),[62] of the standard rate constant value in the absence of thiol monolayer (it should be noted that significantly higher values have recently been reported[43,63] when gold electrodes are used instead of mercury). Though this numerical coincidence may be somewhat fortuitous, due to the uncertainty associated with the graphical extrapolation in Figure 9c and in the definition of the donor−acceptor distance, it implies that the rate of decay of the electronic coupling upon increasing the donor−acceptor distance is likely to persist for a range of rate constants spanning 7 orders of magnitude. It also supports the contention that β

(53) Krysinski, P.; Moncelli, M. R.; Tadini-Buoninsegni, F. *Electrochim. Acta* **2000**, *45*, 1885.
(54) Brown, G. M.; Sutin, N. *J. Am. Chem. Soc.* **1979**, *101*, 883.
(55) Liu, Y.-P.; Newton, M. D. *J. Phys. Chem.* **1994**, *98*, 7162.
(56) Lide, D. R., Ed. *Handbook of Chemistry and Physics*, 71st ed.; CRC Press: Boca Raton, FL, 1990; pp 10−287.
(57) Hupp, J. T.; Weaver, M. J. *J. Phys. Chem.* **1985**, *89*, 2795.
(58) Creager, S. E.; Wooster, T. T. *Anal. Chem.* **1998**, *70*, 4257.
(59) (a) Hsu, C.-P.; Marcus, R. A. *J. Chem. Phys.* **1997**, *106*, 548. (b) Hsu, C.-P. *J. Electroanal. Chem.* **1997**, *438*, 27.
(60) Schmickler, W. *Interfacial Electrochemistry*; Oxford University Press: New York, 1996; p 99.
(61) Gennet, T.; Weaver, M. J. *Anal. Chem.* **1984**, *56*, 1444.
(62) Wipf, D. O.; Kristensen, E. W.; Deakin, M. R.; Wightman, R. M. *Anal. Chem.* **1988**, *60*, 306.
(63) Muzikár, M.; Fawcett, W. R. *Anal. Chem.* **2004**, *76*, 3607.

values for molecular bridges composed of water molecules (the likely molecular bridge between mercury and $Ru(NH_3)_6^{3+}$ in the absence of a thiol monolayer) are similar to those found for covalently linked saturated hydrocarbon spacers.[64]

The facility of non-ionized MUA-coated electrodes (pH 2) to block electron exchange appears to be intermediate between that of MHOL and MUOL monolayers, indicating that carboxylic-terminated monolayers constitute less efficient electronic barriers than their hydroxyl-terminated counterparts. This difference can be ascribed to either a stronger electronic coupling across the carboxylic groups or a shorter tunneling distance due to the penetration of the redox probe into the outer part of the monolayer. The latter explanation seems to be supported by the monolayer permittivity values listed in Table 1, as far as these values are assumed to reflect the ion/water content of the monolayers. However, the involvement of the carboxylic groups in the formation of extended hydrogen-bonded structures should also be considered as a possible source of the enhanced electron transfer rate, since the presence of these supramolecular structures seems to be at the source of the increase in tunneling current between a gold electrode and either a tethered or a freely diffusing redox probe upon incorporation of an amide moiety into alkanethiol monolayers.[11,19]

The electroreduction of $Ru(NH_3)_6^{3+}$ at the MUA-coated Hg electrode in a pH 7 buffer solution deviates from the expected behavior for a simple one-electron process. Thus, values of electron transfer rate constant, derived by assuming first-order reaction kinetics, were found to decrease systematically upon increasing the $Ru(NH_3)_6^{3+}$ concentration in solution (see Figure 9b). Moreover, the transition from exponential-like to peak-shaped voltammograms, as the solution pH was varied from 2 to 7 (Figure 2c), reveals a faster redox process at the negatively charged MUA monolayers. A similar increase of electron transfer rate, from $k_s = 6.3 \times 10^{-3}$ cm s^{-1} at pH 3 to $k_s = 0.13$ cm s^{-1} at pH 7, was also observed in the presence of MPH monolayers[48] (see Table 1 and Figure 9c), though first-order kinetics were obeyed in this case. A detailed analysis of the surface acid/base ionization of these thiol-modified electrodes will be the subject of a future communication, but it may be interesting to mention here that no pH dependence was detected for $Ru(NH_3)_6^{3+}$ reduction at MUOL-coated mercury electrodes.

Soluble redox probes have commonly been used in connection with saturated hydrocarbon thiol monolayers. Figure 9a,c shows a significant increase in electron transfer rate when a phenyl ring (as in MPH) replaces a saturated hydrocarbon chain of similar length (i.e., MBOL) as molecular spacer. Although the high k_s value obtained at pH 7 may be in part the result of a closer approach of the redox probe to the electrode surface, due to a partial ionization of the terminal $-$OH group, the lower k_s value obtained in acidic solutions, where MPH is expected to be in its neutral form, is consistent with $\beta \approx 0.4$ Å^{-1}. This value is similar to that reported for electron transfer through oligophenylene molecular wires.[5d,65,66]

The internal consistency of the kinetic results and their compliance with the theoretical expectations provide strong evidence against the presence of pinholes and defects in the monolayers grown under potentiostatic control. It may be surmised that the lateral mobility of the surface mercury atoms at room temperature facilitates a self-annealing mechanism that helps to restore the structure of the films. A second source of non-ideality in these systems would be the formation of multilayered films. Both the capacitance values listed in Table 1 and the attainment of a limiting reductive charge in the stripping experiments[17,48] argue against the formation of multilayers. Here, the control parameter is the deposition potential, which should be positive enough to drive the thiol oxidation, but not so positive as to destroy the barrier properties of the monolayer.

Concluding Remarks

Self-assembled monolayers provide a means to control charge transfer processes, either by modulating the rate of electron exchange or by blocking ion transfer across the monolayer. In the present work, we have studied the electrochemical stability and blocking properties of several thiol monolayers. The results reveal that ion permeation through ω-functionalized alkanethiol monolayers is a (kinetically) slow process, whose activation energy is strongly influenced by the applied potential and chemical composition of the intervening medium. Experimental evidence for voltage-induced gating of these monolayers was obtained in the form of a chronoamperometric spike, which signals a disordering and partial desorption of the monolayer. Mercaptobutanol and mercaptophenol monolayers preserve their electronic barrier properties with time, whereas mercaptohexanol, mercaptoundecanol, and mercaptoundecanoic acid monolayers undergo an order/disorder transition below a critical potential, which facilitates the approach of the redox species to the electrode surface.

The good correlation between standard rate constant and thickness of hydroxyl-terminated SAMs indicates that on a short time scale the electron transfer plane is located outside the monolayer. In quantitative agreement with Marcus' theory, a leveling off of the activation-energy/driving-force relationship was observed at the higher overpotential values attainable with the longer thiols. Substitution of the hydroxy functionality by a bulkier carboxylic group results in an increase of the electron transfer rate, which might be due to (i) a higher donor/acceptor electronic coupling in the presence of COOH or (ii) a decrease of the tunneling distance due to penetration of the redox probe into the outer part of the monolayer. Finally, replacement of the saturated hydrocarbon thiol chain by a delocalized π-electron phenyl group has been shown to lead to a significant increase of the electron transfer rate.

Overall, the proposed electrochemical protocol for in situ formation and probing of thiol monolayers appears to be a convenient tool for investigating the interplay between long-range electron transfer and redox probe permeation processes across self-assembled monolayers. It enables one to create the experimental conditions under which accurate information on the electronic conducting properties of molecular wires can be obtained.

Acknowledgment. This work was supported by the Spanish DGICYT under Grant BQU2002-02603.

JA050265J

(64) Newton, M. D. *J. Electroanal. Chem.* **1997**, *438*, 3.
(65) Creager, S.; Yu, C. J.; Bamdad, C.; O'Connor, S.; MacLean, T.; Lam, E.; Chong, Y.; Olsen, G. T.; Luo, J.; Gozin, M.; Kayyem, J. F. *J. Am. Chem. Soc.* **1999**, *121*, 1059.
(66) Sikes, H. D.; Smalley, J. F.; Dudek, S. P.; Cook, A. R.; Newton, M. D.; Chidsey, C. E. D.; Feldberg, S. W. *Science* **2001**, *291*, 1519.